Anti-Tumor Effect via Passive Anti-angiogenesis of PEGylated Liposomes Encapsulating Doxorubicin in Drug Resistant Tumors

Golam Kibria, Hiroto Hatakeyama, Yusuke Sato, Hideyoshi Harashima*

Laboratory of Innovative Nanomedicine, Faculty of Pharmaceutical Sciences,
Hokkaido University, Kita 12 Nishi 6, Kita-ku, Sapporo 060-0812, Japan

*Corresponding author:
Hideyoshi Harashima, Professor
Faculty of Pharmaceutical Sciences
Hokkaido University
Sapporo, Hokkaido, 060-0812, Japan.
Tel.: +81 11 706 3919, Fax: +81 11 706 4879.
E-mail: harasima@pharm.hokudai.ac.jp

Abstract

The PEGylated liposomal (PEG-LP) Doxorubicin, PEG-LP (DOX), with a diameter of around 100 nm, accumulates in tumors via the enhanced permeability and retention (EPR) effect, and is used clinically for the treatment of several types of cancer. However, there are a number of tumor types that are resistant to DOX. We report herein on a unique anti-tumor effect of PEG-LP (DOX) in a DOX-resistant tumor xenograft model. PEG-LP (DOX) failed to suppress the growth of the DOX-resistant tumors (ex. non-small cell lung cancer, H69AR; renal cell carcinoma, OSRC-2) as observed in the xenograft model. Unexpectedly, tumor growth was suppressed in a DOX-resistant breast cancer (MDA-MB-231) xenograft model. We investigated the mechanism by which PEG-LP (DOX) responses differ in different drug resistant tumors. In hyperpermeable OSRC-2 tumors, PEG-LP was distributed to deep tumor tissues, where it delivers DOX to drug-resistant tumor cells. In contrast, extracellular matrix (ECM) molecules such as collagen, pericytes, cancer-associated fibroblasts make the MDA-MB-231 tumors hypopermeable, which limits the penetration and distribution of PEG-LP, and thereby enhances the delivery of DOX around the tumor vasculature. Therefore, a remarkable anti-angiogenic effect with a preferential suppression in tumor growth is achieved. Based on the above findings, it appears that the response of PEG-LP (DOX) to drug-resistant tumors results from differences in the tumor microenvironment.

Keywords

PEGylated liposome, Doxil, Drug-resistant cancer, Passive anti-angiogenesis, Anti-tumor effect

1. Introduction

Chemotherapy, using several cytotoxic drugs including doxorubicin (DOX), is one of major therapeutic approaches to the clinical treatment of cancers. However, the major obstacle to the effective treatment of cancer is associated with the fact that cancer cells eventually become resistant to chemotherapy, a phenomenon that is commonly called cancer multidrug resistance (MDR) (Desoize and Jardillier, 2000; Goldie, 2001; Niero et al., 2014). Despite the strong cytotoxic effect, the unequal biodistribution and severe adverse effects on normal healthy tissues (Swain et al., 2003) as well as the resistance of cancer cells limits the application of chemotherapeutic drugs in clinics. Nanoparticles loaded with such drugs have the ability to bypass the factors responsible for the MDR of cancer cells to the free drug molecules, thereby are able to function more effectively against the MDR cancers (Arora et al., 2012; Markman et al., 2013). Moreover, ligand modified targeted nanoparticles are also utilized to overcome the MDR of cancer cells to chemotherapy (Kibria et al., 2013; Qiu et al., 2015; Takara et al., 2012).

In cancer therapy, liposomes (LPs) have become an emerging and effective tool that modifies the pharmacokinetics and distribution of drug molecules, thereby reducing the toxicities associated with the use of chemotherapeutic drugs (Slingerland et al., 2012). Polyethylene glycol (PEG) allows LPs to escape from the mononuclear phagocyte system/reticuloendothelial system (RES), thereby increasing the *in vivo* circulating time as well as the biostability of the LPs (Allen and Cullis, 2013; Bedu-Addo et al., 1996). Due to their long circulation property, PEGylated liposomes (PEG-LPs) are passively extravasated and accumulate in tumor tissues through the leaky tumor vasculature by a universal mechanism referred to as the enhanced permeability and retention (EPR) effect (Fang et al., 2011; Hashizume et al., 2000; Kibria et al., 2013; Maeda, 2012; McDonald and Baluk, 2002). One representative example of such a PEG-LP is Doxil, which was approved by the US Food and Drug Administration (FDA) in 1995. In this preparation, DOX is encapsulated in LPs with surface-bound methoxypolyethyleneglycol 2000 (PEG2000), and the resulting

particles have a diameter of ~100 nm (dnm). They function via the EPR effect against the breast cancer, ovarian cancer and AIDS related Kaposi's sarcoma where the disease has progressed or recurred after platinum-based chemotherapy (Barenholz, 2012; Duggan and Keating, 2011; Immordino et al., 2006; Northfelt et al., 1996; Symon et al., 1999).

Due to its pharmacokinetic characteristics, facilitating tissue accumulation as well as the novel mechanism of accumulation in tumor tissues (Northfelt et al., 1996; Symon et al., 1999), Doxil or PEG-LP (DOX) functions by delivering DOX to tumor tissues, thereby exerting its effects against the tumor cells. On the other hand, DOX delivered by Doxil fails to provide a therapeutic benefit in several other tumor models including the renal cell carcinoma (RCC) (Choi et al., 2013; Kibria et al., 2013; Takara et al., 2012) where the tumor cells are resistant to DOX. It is eventually predicted that cancer cells that are resistant to DOX, cannot be treated by Doxil or PEG-LP (DOX). Therefore, the site of action of the drug delivered by the delivery tool is critical for achieving the expected therapeutic benefit. The mechanisms of resistance of cancer cells to DOX are well identified and have been evaluated (Broxterman et al., 2009; Kibria et al., 2014b) however, the accumulation and distribution pattern of PEG-LP (DOX) in MDR tumor models is not well understood.

In the present study, we present information regarding the unique anti-tumor effect of PEG-LP (DOX) in DOX-resistant tumors. We investigated the therapeutic effect of PEG-LP (DOX) in three different types of tumor models that are resistant to DOX, and explored the mechanism by which PEG-LP (DOX) responds in a different manner in different DOX-resistant tumors.

2. Materials and methods

Hydrogenated soybean phosphatidylcholine (HSPC), N-(lissamine rhodamine B sulfonyl)-1,2-dioleoyl-sn-glycero-3-phosphoethanolamine (rhodamine-DOPE), 1,2-distearoyl-*sn*-glycero-3-phosphoethanolamine-N-[methoxy (polyethyleneglycol)-2000] (PEG2000-DSPE), Cholesterol, Egg phosphatidylcholine (EPC) were purchased from Avanti Polar Lipids (Alabaster, AL, USA). Doxorubicin Hydrochloride was purchased from Wako Pure Chemical Industries (Osaka, Japan). Hoechst 33342 and RPMI 1640 medium were purchased from Dojindo (Tokyo, Japan) and Lonza (Walkersville, MD, USA), respectively.

2.1. Cell cultures

Human breast cancer (MDA-MB-231) ((American Type Culture Collection (ATCC), VA, USA)), small cell lung cancer (H69AR) (ATCC), and renal cell carcinoma (OSRC-2; Riken cell bank, Tsukuba, Japan) cells were cultured in RPMI 1640 medium supplemented with 10% FBS (v/v), penicillin (100 units/ml), streptomycin (100 mg/ml) under an atmosphere of 5% CO_2 at 37°C. Human cervical cancer (Hela; Riken cell bank) cells were cultured in DMEM supplemented with 10% FBS (v/v), penicillin (100 units/ml), streptomycin (100 mg/ml) under the same atmospheric conditions.

2.2. Preparation of DOX loaded PEG-LPs

The lipid film hydration method was also followed to prepare the LPs composed of HSPC:Cholesterol (70:30) as described previously (Kibria et al., 2013). Briefly, the lipid film was hydrated with 155 mM ammonium sulfate for 25 min followed by a probe sonication. DOX in PBS was added to the LPs (drug-to-lipid molar ratio of 1:10) followed by incubation at 60°C for 1 h, and the free DOX was removed by means of an Amicon 50,000 MWCO filter. The amount of DOX in LPs was determined by disintegration of the liposomal bilayer in methanol and colorimetric determination of DOX concentration. The DOX loaded LPs were incubated with 5 mol% PEG2000-DSPE at 60 °C for 30 min to prepare the PEG-LP (DOX).

2.3. Preparation of PEG-LPs for biodistribution study

The lipid film hydration method was used to prepare the PEGylated liposomes (PEG-LPs). A lipid film composed of EPC/Cholesterol/PEG2000-DSPE/rhodamine-DOPE (molar ratio: 70/30/5/1) was formed by evaporation of the organic solvents from the lipid solution in a glass tube. The lipid film was hydrated with the HEPES buffer (10 mM, pH 7.4) followed by sonication for about 30 sec in a bath-type sonicator (AU-25C, Aiwa, Tokyo, Japan).

2.4. Characterization of PEG-LPs

The prepared PEG-LPs were characterized by measuring its mean size and zeta potential using a Zetasizer Nano ZS ZEN3600 instrument (Malvern Instruments Ltd., Worchestershire, UK).

2.5. *In vivo* anti-tumor efficacy

Tumor cells were inoculated on the back of BALB/c nude mice (female mice used for MDA-MB-231 cells, male mice used for H69AR and OSRC-2 cells). DOX loaded PEG-LPs were injected into tumor (at a tumor volume of ~150 mm^3) bearing mice (n=4-5) via tail vein with a once daily dose of 2 mg DOX (either free or in PEG-LP)/kg body weight or with PBS (control) at days 1, 4, 7 and day 10. Body weights and tumor volumes were monitored at three day intervals. Tumor volume was calculated using the formula: 1/2 x a x b^2, where a and b represent the largest and smallest diameters of tumors, respectively. All animal experiments were performed according to the national regulations and approved by the Hokkaido University Animal Care Committee.

2.6. Detection of cell cytotoxicity

The effect of free DOX on the viability of cells was determined by the WST-8 assay protocol, as described previously (Kibria et al., 2013). Briefly, 4,000 cells were plated in 96-well plate and incubated overnight. The next day, the cells were incubated with different doses of DOX for 8 h at 37°C, followed by reincubation for

16 h in the presence of fresh media. After washing with PBS, cells were re-incubated with a cell counting kit-8 (CCK-8) solution (Dojindo) for 2 h and the absorbance of the developed color was measured at 450 nm using a microplate reader (Thermo Fisher Scientific Inc.). The same protocol was followed to compare the cytotoxic effect of free DOX and DOX loaded PEG-LPs on the viability of MDA-MB-231 cells. In this case, the cells were incubated with different concentrations of DOX (as free drug or encapsulated within the PEG-LPs) at 37°C for 8 h, followed by reincubation for 16 h in the presence of fresh media.

2.7. Observation of cell morphology *in vitro*

To observe morphological changes of MDA-MB-231, 40,000 cells were seeded on a 35-mm glass-bottom dish for 24 h. Next day, cells were incubated with 20 μg/ml of DOX (as free drug or encapsulated within the PEG-LPs) in cell culture media for 30 h at 37°C. After 30 h, the media was removed followed by washing with PBS and were observed under confocal laser scanning microscopy, CLSM (Nikon A1, Nikon Instruments Inc., Tokyo, Japan).

2.8. Time dependent cytosolic distribution of DOX

To observe the distribution of DOX, 40,000 cells were seeded on a 35-mm glass-bottom dish. On the next day, 50 μg/ml of DOX (as the free drug or encapsulated within the PEG-LPs) in cell culture media was added to the cells and incubated for 3 h at 37°C. At 2.5 h, cells nuclei were labeled with Hoechst 33342 for 30 min. At 3 h, the previous medium was removed followed by washing with PBS and fresh medium was added and the samples were reincubated for an additional 20 h, followed by washing with PBS and fresh medium was added, followed by reincubation for an additional 32 h. Images at 3 h, 23 h and 55 h time points were taken by CLSM.

2.9. Quantification of mRNA expression

When tumor sizes reached a volume of 100 to 200 mm^3, tumor tissues were collected. Samples containing approximately 30 mg of tumor tissues were homogenized using a Precellys 24 (Birthin technologies, Montigny-le-Bretonneux, France) in 500 μL of TRI_{ZOL} reagent (Ambion, Austin, TX). Total RNA was extracted according to manufacturer's protocol. The total RNA (1 μg) was reverse transcribed using a High Capacity RNA-to-cDNA kit (Applied Biosystems, Carlsbad, CA, USA) according to manufacturer's protocol. A quantitative PCR analysis was performed on 2 ng cDNA using Fast SYBR Green Master Mix (Applied Biosystems) and Lightcycler 480 system II (Roche Diagnostics GmbH, Germany). All reactions were performed at a volume of 15 μL. The primers for mouse GAPDH were (forward) 5'-AGC AAG GAC ACT GAG CAA G-3' and (reverse) 5'-TAG GCC CCT CCT GTT ATT ATG-3', for mouse CD31 (vascular endothelial cell marker) were (forward) 5'-TAC AGT GGA CAC TAC ACC TG-3' and (reverse) 5'-GAC TGG AGG AGA ACT CTA AC', for mouse NG2 (pericyte marker) were (forward) 5'-AAG GAA GTG CAG AGG AG-3' and (reverse) 5'-CAT CTC GTG CTC ATA CAG-3', for mouse Col1a1 (collagen type 1 marker) were (forward) 5'-AGA GAG GTG AAC AAG GTC-3' and (reverse) 5'-AAG GTC TCC AGG AAC AC-3', for mouse Pdgfrb (platelet-derived growth factor receptor protein) were (forward) 5'-GTG ATA GCT CAC ATC AGA AG-3' and (reverse) 5'-ATA ACA CGG ACA GCA AC-3' and for mouse Fapα (fibroblast marker) were (forward) 5'-CCA GTT CCA GAA ATG ATA GCC-3' and (reverse) 5'-GAC AGG ACT GAG ACA TTC TGC-3'.

2.10. *In vivo* distribution of PEG-LPs in the tumor tissues

Mice bearing the MDA-MB-231 tumors (~150 mm^3) were injected with rhodamine-labeled PEG-LPs (1.0 μmol lipid/200 μl). At 23.5 h post-injection, FITC-conjugated griffonia simplicifolia isolectin B4 (GS-IB4-FITC) (Vector Laboratories Inc.) was injected via tail vein to stain the blood vessels. After 30 min, mice were sacrificed and tumors were collected and frozen in Optimal Cutting Temperature (OCT) compound under liquid nitrogen. The frozen tissues were further sectioned

(thickness, 10 μm) in a cryostat, fixed on a glass slide followed by observation under a microscope (CLSM).

2.11. Detection of cell apoptosis *in vivo*

The MDA-MB-231 tumor bearing mice (tumor volume ~100 mm^3) were injected with 3 mg DOX/kg body weight at days 1 and 4. At day 5, 200 μl of Apo-Trace solution was injected via tail vein and incubated for 2 h. Mice were anesthetized, tumors were collected and incubated with Alexa Fluor 647-Isolectin (GS-IB4) solution (Invitrogen) to stain the blood vessels followed by CLSM analysis. The area of the blood vessels in each confocal image of the tumors was calculated by counting the total number of pixels using ImagePro-plus software.

2.12. Statistical analysis

Data was expressed as mean ± standard deviation. Pair-wise comparisons of subgroups were made following the two-tail Unpaired Student *t*-test. Differences among means were considered to be statistically significant at a p value of ≤0.01 and ≤0.05.

3. Results

3.1. *In vivo* anti-tumor effect of DOX and PEG-LP (DOX)

We first evaluated the anti-tumor activity of DOX and the DOX encapsulating PEG-LP ((PEG-LP (DOX); size: 105±4.1 nm in diameter, zeta-potential: -12.6±2.2 mV, polydispersity index (PDI): 0.151, DOX encapsulation efficiency: >96%; where the commercially available PEG-LP (DOX), Doxil; size: 108 nm, zeta-potential: -13.3 mV, DOX encapsulation efficiency: >95%; Gabizon et al., 2003; Szebeni et al., 2012)) in mice bearing MDA-MB-231 and H69AR tumors which are known to be resistant to DOX (Fig. 1). Mice were intravenously injected with either free DOX or PEG-LP (DOX) at a DOX dose of 2 mg/kg at the indicated time points. Free DOX failed to induce a detectable anti-tumor effect in mice bearing MDA-MB-231 tumors (Fig. 1A-B). Unexpectedly, PEG-LP (DOX) showed a significant suppression of tumor growth in the MDA-MB-231 xenograft model for up to 30 days after the first injection (Fig. 1C-D). On the other hand, PEG-LP (DOX) failed to suppress tumor growth in the H69AR xenograft model (Fig. 1E-F). The inefficiency of PEG-LP (DOX) in inhibiting tumor growth was also observed in mice bearing the OSRC-2 tumors, as previously reported (Kibria et al., 2013). These results indicate that DOX loaded PEG-LP ((PEG-LP (DOX)) has a different therapeutic effect than free DOX in different tumor types despite the fact that they are resistant to DOX.

3.2. Response of tumor cells to DOX

We further assessed the sensitivity of MDA-MB-231 to DOX by incubating the cells with free DOX, and compared its effect with that of Hela cells as a sensitive tumor cell model. As shown in Fig. 2, the MDA-MB-231 cells showed a higher IC_{50} value (22.37±7.57 μg/ml) as compared to Hela cells (0.01±0.001 μg/ml). Based on these results as well as on our recent report (Kibria et al., 2014a), it can be concluded that MDA-MB-231 cells can be classified as being resistant to DOX. We also reported that H69AR and OSRC-2 cells are resistant to DOX in our recent study (Kibria et al., 2014a), where the calculated IC_{50} values for those cells were 71.15±52.84 μg/ml and 41.42±27.75 μg/ml, respectively.

3.3. Comparison of the *in vitro* cytotoxic effect of free DOX and liposomal DOX

To examine the mechanism by which anti-tumor effect was induced by treatment with PEG-LP (DOX) in the MDA-MB-231 tumor model, we first compared the *in vitro* cytotoxicity of PEG-LP (DOX) with free DOX whether or not PEG-LP (DOX) enhanced the cytotoxicity of DOX in MDA-MB-231 cells as compared to free DOX. As shown in Fig. 3A, PEG-LP (DOX) was less effective in killing the tumor cells than free DOX. The IC_{50} values of PEG-LP (DOX) and free DOX were found to be 191.24±106.72 μg/ml and 10.74±5.39 μg/ml, respectively.

3.4. Observation of the morphology of cells treated with free DOX and liposomal DOX

To observe the effect of DOX on the morphology of cells, we incubated the MDA-MB-231 cells with free DOX or with DOX loaded PEG-LP, as shown in Fig. 3B. A huge amount of DOX was detected inside the cells that had been treated with a higher dose of drug, and the morphology of cells had changed, becoming round (Fig. 3B), indicating that free DOX shows its cytotoxic effect on the DOX-resistant MDA-MB-231 cells. Compared to free DOX, no change in the shape of the cells was observed when the cells were treated with PEG-LP (DOX), indicating that PEG-LP (DOX) is inefficient in inducing a cytotoxic effect in an *in vitro* environment.

3.5. Intracellular distribution of PEG-LPs (DOX)

To observe and compare the distribution of DOX in various cellular compartments in response to time, MDA-MB-231 cells were incubated with either free DOX or PEG-LP (DOX). A huge amount of free DOX that had accumulated into cells within a 3 h incubation period was detected in the nuclei of cells even after a 55 h culture period (Fig. 4). Compared to free DOX, the amount of DOX delivered at the 3 h time point by PEG-LP (DOX) was substantially lower, and the signals corresponding to DOX in the nuclei were reduced gradually with passing time.

3.6. Evaluation of gene expression

Based on the results presented in Fig. 3 and Fig. 4, it appears that the *in vitro* effect of PEG-LP (DOX) on MDA-MB-231 cancer cells itself cannot be used to explain the *in vivo* anti-tumor effect of PEG-LP (DOX) in mice bearing the MDA-MB-231 xenografts (Fig. 1C-D). Therefore to explore the difference in the *in vivo* tumor microenvironment, we evaluated the expression of different genes in the MDA-MB-231 tumor tissues (Fig. 5), and the results were compared with those of the OSRC-2 tumors, since PEG-LP (DOX) is ineffective against this tumor model (Kibria et al., 2013; Takara et al., 2012). Based on the results presented in Fig. 5A, the expression of the *CD31* gene is 2-fold lower in MDA-MB-231 tumors as compared to that of OSRC-2 tumors, indicating that the MDA-MB-231 tumor is less angiogenic than the OSRC-2 tumor. Additionally, as compared to OSRC-2 tumors, the expressions of pericytes (*NG2*, normalized by *CD31*) and *Pdgfrb* markers were found to be 2-3 fold higher in MDA-MB-231 tumors (Fig. 5A-B), indicating that the MDA-MB-231 tumors are hypopermeable. These results suggest that MDA-MB-231 tumors are less angiogenic and more hypopermeable than the OSRC-2 tumors. Furthermore, the mRNA expression levels of several other genes including *Col1a1* (ECM) and *Fapa* (fibroblast markers) in MDA-MB-231 tumors were also found to be approximately 2-3 fold higher than those in the OSRC-2 tumors (Fig. 5A), suggesting that the MDA-MB-231 tumors have a stroma rich environment as compared to the OSRC-2 tumors. These results indicate that PEG-LP (DOX) is capable of penetrating into the deep tissues of the OSRC-2 tumors, while the penetration of PEG-LP (DOX) would be more limited in the MDA-MB-231 tumors. These results suggest that the presence of extracellular matrix compounds in MDA-MB-231 tumors is responsible for limiting the penetration and distribution of PEG-LPs (i.e. Doxil) deep into tumor tissues.

3.7. Mechanism responsible for the enhanced anti-tumor effect in vivo MDA-MB-231 tumor by PEG-LP (DOX)

To examine our hypothesis, we further observed the distribution of PEG-LP labeled with fluorescence in the tumor tissues. Compared to the control, a huge amount of PEG-LP was detected in the tumor, and where PEG-LP was found around the blood vessels in the MDA-MB-231 tumor after i.v. injection (Fig. 6A). It is well known that PEG-LP passively accumulates in tumors via the EPR effect after intravenous administration (Fang et al., 2011; Kibria et al., 2013; Maeda, 2012). Based on the images presented in Fig. 6A, it is likely that PEG-LP was directed to and accumulated in the tumor tissues via the EPR effect, however, a large population of the PEG-LP was present around the tumor blood vessels and it is possible that a few might reach the tumor cells, given their concentrations. On the other hand, in OSRC-2 tumors, most of the PEG-LPs that accumulated in the tumor were extravasated and directed into deep tumor cells (Fig. 6B and Fig. S1), as we observed in a previous study (Kibria et al., 2013). Taking these results into consideration, it appears that PEG-LP (DOX) is unable to access the tumor cells in MDA-MB-231 tumor tissues, but accumulates in the pre-vasculature region where it might kill tumor endothelial cells and induce the anti-angiogenic effect.

To further explore the effect of PEG-LP (DOX) in more depth, we evaluated the apoptosis of cells in the tumor microenvironment after the administration of PEG-LP (DOX) (Fig. 7). Almost no signals corresponding to apoptotic cells were detected in the MDA-MB-231 tumor treated with the free DOX. In contrast, a huge number of cells undergoing apoptosis were detected in the tumor that had been treated with PEG-LP (DOX), and most of the detected apoptosis signals were merged along with the area of the tumor blood vessels. In addition, compared to the control or the free DOX, signals for the tumor blood vessels were dramatically reduced in number in the case of the tumor treated with PEG-LP (DOX) (Fig. 7A), which is also evident in the quantitative analysis showing a significant level of reduction in the area of the blood vessels (Fig. 7B). These results suggest that the anti-tumor effect of PEG-LP

(DOX) in MDA-MB-231 tumors could be caused by disrupting the blood vessels induced by PEG-LP (DOX), resulting in an anti-angiogenesis effect shutting off the supply of oxygen and nutrients, thus suppressing tumor growth.

4. Discussion

The distribution of nanoparticles in tumor tissues depends on the characteristics of the tumor microenvironment after passively accumulating in the tumor via a process called the EPR effect. It was reported that nanoparticles with diameters in excess of 50 nm hardly penetrate into interstitial rich tumors such as pancreatic cancer (Cabral et al., 2011). The molecular weight and size dependent accumulation of dextran (3.3 kDa-2 MDa) was observed in human squamous cell carcinoma xenograft tissues (Dreher et al., 2006). The tumor vasculatures are much leakier (~100-600 nm) (Hashizume et al., 2000; McDonald and Baluk, 2002) than those of the normal tissues, therefore, it would be much easier for PEG-LPs (~100 nm) to extravasate to tumor cells.

In general, the tumor blood vessel targeted delivery of cargos could be achieved by installing active targeting ligands on the surface of the delivery vehicles. The findings reported herein show that DOX loaded PEG-LP ((PEG-LP (DOX)) having ~100 nm passively accumulated in the tumor vessels followed by the induction of anti-angiogenesis in the tumor microenvironment. Here, we examined three different tumor models, all of which are resistant to DOX. Following the EPR effect, PEG-LP (DOX) accumulates in the tumor tissues, thereby delivering the DOX to the tumor cells. Hence, it is reasonable to predict that PEG-LP (DOX) should not induce an anti-tumor effect in DOX-resistant tumors. To evaluate this assumption, we observed the anti-tumor effect of PEG-LP (DOX) in mice bearing MDA-MB-231 and H69AR tumors. Surprisingly, PEG-LP (DOX) exhibited a remarkable anti-tumor effect in mice bearing the MDA-MB-231 tumors (Fig. 1A), where the free DOX failed to provide any detectable therapeutic effect. On the other hand, no anti-tumor effect of PEG-LP (DOX) was observed in mice bearing H69AR tumors (Fig. 1C), and similarly, PEG-LP (DOX) was also observed to be inefficient in mice bearing OSRC-2 (RCC) tumors, as we reported recently (Kibria et al., 2013; Takara et al., 2012).

To explore the mechanism of action of DOX loaded PEG-LP, PEG-LP (DOX), in DOX-resistant MDA-MB-231 tumors, we first compared the *in vitro* cytotoxic effect of PEG-LP (DOX) with that of the free DOX in MDA-MB-231 cells (Fig. 3A). It was observed that the free DOX exhibited a better cytotoxic effect and a change in the morphology of the cells as compared to that of PEG-LP (DOX) in an *in vitro* situation (Fig. 3). Consequently, we explored the intracellular distribution of PEG-LP (DOX) as a function of time, as indicated in Fig. 4. After a 3 h incubation, a huge amount of free DOX was detected in MDA-MB-231 cells as compared to that of DOX delivered by PEG-LP (DOX). With passing time, the DOX signal in cells that had been treated with free DOX was clearly observed in the nuclei of cells where the DOX actually functions (Fig. 4), due to which free DOX exhibited a better cytotoxic effect and change in cell morphology as compared to PEG-LP (DOX) in an *in vitro* situation (Fig. 3). Moreover, the confocal microscope images suggested that the uptake amount of DOX by PEG-LP (DOX) was lower than that of free DOX (Fig. 4). While free DOX can be readily taken up by the cells, the accumulation of DOX depends on the amount of PEGylated liposomes that is taken up in the case of PEG-LP (DOX) (Fig. 4). Therefore, the lower uptake of DOX delivered by PEG-LP (DOX) could account for the inferior cytotoxicity of PEG-LP (DOX) compared to that of free DOX (Fig. 3). These results indicate that the *in vivo* therapeutic effect of PEG-LP (DOX) (Fig. 1) in MDA-MB-231 breast tumors cannot be explained by its effect observed in the *in vitro* studies (Fig. 3 and Fig. 4).

Therefore, we hypothesized that the difference in anti-tumor effects of PEG-LP (DOX) between the MDA-MB-231 tumor and PEG-LP (DOX)-ineffective tumors (ex. H29AR and OSRC-2), might result from differences in the tumor microenvironment. To explore this further, we evaluated the expression of different genes associated with the extracellular matrix (ECM) molecules (Fig. 5A) in the tumors. Compared to OSRC-2 tumors, the expression of pericytes or other ECM molecules in MDA-MB-231 tumors was found to be significantly higher (Fig. 5A-B). These results demonstrate that the MDA-MB-231 tumors are stroma rich and their vasculatures

are hypopermeable. To explore the effect of the ECM proteins on the penetration of PEG-LP into DOX-resistant tumor tissues, we further evaluated the distribution of PEG-LP (~100 nm) in the tumor microenvironment. Interestingly, based on the results of the biodistribution study (Fig. 6A), most of the PEG-LP was extravasated via the EPR effect, accumulates and resides in close proximity to the blood vessels of the MDA-MB-231 tumor. Therefore, the limited penetration and accumulation of PEG-LP in the MDA-MB-231 tumor further demonstrates its hypopermeable characteristics. Such an observation was also supported by the fact that most of the DOX injected and delivered by the PEG-LP was found in the vicinity of tumor blood vessels (Fig. 7A). Due to such an effect, DOX loaded PEG-LP ((PEG-LP (DOX)) induced apoptosis (Fig. 7A) of the cells present around the tumor blood vessels including tumor endothelial cells (TECs) (Fig. 7A), resulting in the disruption of the tumor blood vessels, and finally inducing a significant anti-angiogenic effect (Fig. 7B and Fig. 8). It is well established that angiogenesis of tumor blood vessels plays a pivotal role in the growth and progression of tumors (Folkman, 1971, 2007). Moreover, in tumor tissues, the growth and survival of tumor cells depends on life support (blood, oxygen, nutrients, growth factors etc.) supplied by the TECs present in the tumor blood vessels. In the case of tumor tissue, the percentage of ECs is very low (~2%), and the number of tumor cells is about 100-times higher as compared to ECs (Folkman, 1995; Matsuda et al., 2010). It can be predicted that the killing of one TEC by the drug molecule would lead to the suppression of growth or even the death of many surrounding tumor cells (Hida et al., 2008; Molema et al., 1998). Therefore, it is reasonable to conclude that the anti-tumor effect of PEG-LP (DOX) in the DOX-resistant MDA-MB-231 tumor (Fig. 1C-D) is mediated by the anti-angiogenic effect of PEG-LP (DOX) (Fig. 8).

On the other hand, compared to MDA-MB-231 tumors, a significantly higher expression of the *CD31* gene was found in the OSRC-2 (RCC) tumors (Fig. 5A), indicating its hypervascular properties, and this observation is consistent with the previous reports showing that RCC tumors are highly angiogenic (Iwai et al., 2004;

Kaelin, 2004). Moreover, the blood vessels of OSRC-2 tumors were found very leaky or hyperpermeable (Fig. 6B and Fig. S1) (Kibria et al., 2013), this was also supported by the presence of comparatively lower levels of extracellular matrix proteins (Fig. 5). Hence, the leakiness of OSRC-2 tumor vasculatures dictates the accumulation of PEG-LP (DOX) in deep tumor tissues where the tumor cells are resistant to DOX (Fig. 8). Therefore, in OSRC-2 tumors, apoptotic cells were nearly absent in the tumor treated with the PEG-LP (DOX) (Fig. S2). Moreover, no anti-angiogenic effect of PEG-LP (DOX) was observed in OSRC-2 tumors, indicating that PEG-LP (DOX) fails to induce blood vessel disruption (Fig. S3), and, as a result, has negligible therapeutic effect (Kibria et al., 2013) (Fig. 8). Similar to the OSRC-2 tumor, the H69AR tumor would be predicted to show a similar distribution and accumulation pattern of PEG-LP, which might lead to the failure of PEG-LP (DOX) against the DOX-resistant H69AR tumor cells (Fig. 1E-F).

Although the EPR effect enhances the accumulation and localization of nanoparticles in the solid tumors, the presence of extracellular matrix (ECM) molecules such as collagen (McKee et al., 2006; Provenzano et al., 2006; Stylianopoulos et al., 2012), pericytes (Hida et al., 2008), cancer-associated fibroblasts (Stylianopoulos et al., 2012) in tumors form a barrier that limits the penetration and distribution of nanoparticles through the interstitial space. The intrinsic barriers drastically affect the anti-tumor efficacy of nanoparticles by impairing their penetration and the subsequent delivery of drug molecules in the tumors. Therefore, degradation of the matrix (Cabral et al., 2011; Jacobetz et al., 2013; McKee et al., 2006; Stylianopoulos et al., 2012) and the depletion of cancer-associated fibroblasts (Chauhan et al., 2013; Stylianopoulos et al., 2012) decompress the tumor vessels, and preferentially enhance the delivery, distribution and therapeutic efficacy of the drug molecules by the nanoparticles. However, such intrinsic barriers likely play a pivotal role in the passive accumulation of PEG-LP (DOX) around the vasculatures of MDA-MB-231 tumor tissues (Fig. 6A and Fig. 7), and the subsequent delivery of DOX disrupts the tumor vasculature, eventually

resulting in an anti-angiogenic effect. Such a process would induce a significant anti-tumor effect for PEG-LP (DOX) in DOX resistant MDA-MB-231 tumors. However, in an *in vitro* study, due to the higher cellular uptake of free DOX, the cytotoxic effect on MDA-MB-231 cells was enhanced, as compared to PEG-LP (DOX), indicating that the *in vitro* results for PEG-LP (DOX) do not explain the outcome of its effect *in vivo*. Taken together our results indicate that, depending on the penetration and accumulation pattern of the PEG-LP in the tumor tissue, a PEG-LP loaded with a drug would be capable of exerting a therapeutic effect against tumors in which the tumor cells are drug-resistant.

5. Conclusions

In the tumor micro-environment, the intrinsic barriers created by the presence of extracellular matrix (ECM) molecules govern the penetration and distribution of PEG-LP in the tumors. In this study, PEG-LP (DOX), DOX encapsulated within a PEG-LP, showed an efficient anti-tumor effect in multidrug resistant (MDR) breast cancer (MDA-MB-231) xenograft model. Due to the hypopermeable characteristics of the MDA-MB-231 tumors, PEG-LP accumulates around the tumor vasculature as the result of the EPR effect, and the DOX delivered by the PEG-LP preferentially induces an anti-angiogenic effect, thereby causing the angiogenesis dependent inhibition of DOX resistant tumor growth. In contrast, due to the presence of PEG-LP in the deep tissues of hyperpermeable MDR renal cell carcinoma (OSRC-2) tumors, PEG-LP (DOX) fails to induce anti-angiogenesis as well as an anti-tumor effect. Our study demonstrated that the ECM molecules preferentially limit the penetration and accumulation of nanoparticles around the tumor vasculature and such an effect contributes to the therapeutic efficacy of drug loaded nanoparticles in MDR tumors. To overcome the limitations associated with the MDR in cancer, the site of action of the drug delivered by the nanoparticles in the microenvironment of the MDR tumors is critical and clearly needs to be elucidated for the development of an effective drug delivery system for the treatment of MDR cancers in the future.

Acknowledgments

This work in part supported by grants from the Special Education and Research Expenses of the Ministry of Education, Culture, Sports, Science and Technology of Japan (MEXT); and the Nagai Foundation, Tokyo.

References

Allen, T.M., Cullis, P.R., 2013. Liposomal drug delivery systems: from concept to clinical applications. Adv. Drug Deliv. Rev. 65, 36-48.

Arora, H.C., Jensen, M.P., Yuan, Y., Wu, A., Vogt, S., Paunesku, T., Woloschak, G.E., 2012. Nanocarriers enhance Doxorubicin uptake in drug-resistant ovarian cancer cells. Cancer Res. 72, 769-778.

Barenholz, Y., 2012. Doxil(R)--the first FDA-approved nano-drug: lessons learned. J. Control. Release 160, 117-134.

Bedu-Addo, F.K., Tang, P., Xu, Y., Huang, L., 1996. Effects of polyethyleneglycol chain length and phospholipid acyl chain composition on the interaction of polyethyleneglycol-phospholipid conjugates with phospholipid: implications in liposomal drug delivery. Pharm. Res. 13, 710-717.

Broxterman, H.J., Gotink, K.J., Verheul, H.M., 2009. Understanding the causes of multidrug resistance in cancer: a comparison of doxorubicin and sunitinib. Drug Resist. Update. 12, 114-126.

Cabral, H., Matsumoto, Y., Mizuno, K., Chen, Q., Murakami, M., Kimura, M., Terada, Y., Kano, M.R., Miyazono, K., Uesaka, M., Nishiyama, N., Kataoka, K., 2011. Accumulation of sub-100 nm polymeric micelles in poorly permeable tumours depends on size. Nat. Nanotechnol. 6, 815-823.

Chauhan, V.P., Martin, J.D., Liu, H., Lacorre, D.A., Jain, S.R., Kozin, S.V., Stylianopoulos, T., Mousa, A.S., Han, X., Adstamongkonkul, P., Popovic, Z., Huang, P., Bawendi, M.G., Boucher, Y., Jain, R.K., 2013. Angiotensin inhibition enhances drug delivery and potentiates chemotherapy by decompressing tumour blood vessels. Nat. Commun. 4, 2516.

Choi, I.K., Strauss, R., Richter, M., Yun, C.O., Lieber, A., 2013. Strategies to increase drug penetration in solid tumors. Front. Oncol. 3, 193.

Desoize, B., Jardillier, J., 2000. Multicellular resistance: a paradigm for clinical resistance? Crit. Rev Oncol. Hematol. 36, 193-207.

Dreher, M.R., Liu, W., Michelich, C.R., Dewhirst, M.W., Yuan, F., Chilkoti, A., 2006. Tumor vascular permeability, accumulation, and penetration of macromolecular drug carriers. J. Natl. Cancer Inst. 98, 335-344.

Duggan, S.T., Keating, G.M., 2011. Pegylated liposomal doxorubicin: a review of its use in metastatic breast cancer, ovarian cancer, multiple myeloma and AIDS-related Kaposi's sarcoma. Drugs 71, 2531-2558.

Fang, J., Nakamura, H., Maeda, H., 2011. The EPR effect: Unique features of tumor blood vessels for drug delivery, factors involved, and limitations and augmentation of the effect. Adv. Drug Deliv. Rev. 63, 136-151.

Folkman, J., 1971. Tumor angiogenesis: therapeutic implications. N Engl J Med. 285, 1182-1186.

Folkman, J., 1995. Angiogenesis in cancer, vascular, rheumatoid and other disease. Nat. Med. 1, 27-31.

Folkman, J., 2007. Angiogenesis: an organizing principle for drug discovery? Nat Rev Drug Discov. 6, 273-286.

Gabizon, A., Shmeeda, H., Barenholz, Y., 2003. Pharmacokinetics of pegylated liposomal Doxorubicin: review of animal and human studies. Clin Pharmacokinet. 42, 419-36.

Goldie, J.H., 2001. Drug resistance in cancer: a perspective. Cancer Metastasis Rev. 20, 63-68.

Hashizume, H., Baluk, P., Morikawa, S., McLean, J.W., Thurston, G., Roberge, S., Jain, R.K., McDonald, D.M., 2000. Openings between defective endothelial cells explain tumor vessel leakiness. Am J Pathol. 156, 1363-1380.

Hida, K., Hida, Y., Shindoh, M., 2008. Understanding tumor endothelial cell abnormalities to develop ideal anti-angiogenic therapies. Cancer Sci. 99, 459-466.

Immordino, M.L., Dosio, F., Cattel, L., 2006. Stealth liposomes: review of the basic science, rationale, and clinical applications, existing and potential. Int. J. Nanomedicine 1, 297-315.

574 Iwai, A., Fujii, Y., Kawakami, S., Takazawa, R., Kageyama, Y., Yoshida, M.A.,
575 Kihara, K., 2004. Down-regulation of vascular endothelial growth factor in
576 renal cell carcinoma cells by glucocorticoids. Mol. Cell. Endocrinol. 226, 11-17.
577 Jacobetz, M.A., Chan, D.S., Neesse, A., Bapiro, T.E., Cook, N., Frese, K.K., Feig, C.,
578 Nakagawa, T., Caldwell, M.E., Zecchini, H.I., Lolkema, M.P., Jiang, P., Kultti,
579 A., Thompson, C.B., Maneval, D.C., Jodrell, D.I., Frost, G.I., Shepard, H.M.,
580 Skepper, J.N., Tuveson, D.A., 2013. Hyaluronan impairs vascular function
581 and drug delivery in a mouse model of pancreatic cancer. Gut 62, 112-120.
582 Kaelin, W.G., Jr., 2004. The von Hippel-Lindau tumor suppressor gene and kidney
583 cancer. Clin. Cancer Res. 10, 6290S-6295S.
584 Kibria, G., Hatakeyama, H., Akiyama, K., Hida, K., Harashima, H., 2014a.
585 Comparative study of the sensitivities of cancer cells to doxorubicin, and
586 relationships between the effect of the drug-efflux pump P-gp. Biol. Pharm.
587 Bull. 37, 1926-1935.
588 Kibria, G., Hatakeyama, H., Harashima, H., 2014b. Cancer multidrug resistance:
589 mechanisms involved and strategies for circumvention using a drug delivery
590 system. Arch. Pharm. Res. 37, 4-15.
591 Kibria, G., Hatakeyama, H., Ohga, N., Hida, K., Harashima, H., 2013. The effect of
592 liposomal size on the targeted delivery of doxorubicin to Integrin
593 alphavbeta3-expressing tumor endothelial cells. Biomaterials 34, 5617-5627.
594 Maeda, H., 2012. Macromolecular therapeutics in cancer treatment: the EPR effect
595 and beyond. J. Control. Release 164, 138-144.
596 Markman, J.L., Rekechenetskiy, A., Holler, E., Ljubimova, J.Y., 2013.
597 Nanomedicine therapeutic approaches to overcome cancer drug resistance.
598 Adv. Drug Deliv. Rev. 65, 1866-1879.
599 Matsuda, K., Ohga, N., Hida, Y., Muraki, C., Tsuchiya, K., Kurosu, T., Akino, T.,
600 Shih, S.C., Totsuka, Y., Klagsbrun, M., Shindoh, M., Hida, K., 2010. Isolated
601 tumor endothelial cells maintain specific character during long-term culture.
602 Biochem. Biophys. Res. Commun. 394, 947-954.

McDonald, D.M., Baluk, P., 2002. Significance of blood vessel leakiness in cancer. Cancer Res. 62, 5381-5385.

McKee, T.D., Grandi, P., Mok, W., Alexandrakis, G., Insin, N., Zimmer, J.P., Bawendi, M.G., Boucher, Y., Breakefield, X.O., Jain, R.K., 2006. Degradation of fibrillar collagen in a human melanoma xenograft improves the efficacy of an oncolytic herpes simplex virus vector. Cancer Res. 66, 2509-2513.

Molema, G., Meijer, D.K., de Leij, L.F., 1998. Tumor vasculature targeted therapies: getting the players organized. Biochem. Pharmacol. 55, 1939-1945.

Niero, E.L., Rocha-Sales, B., Lauand, C., Cortez, B.A., de Souza, M.M., Rezende-Teixeira, P., Urabayashi, M.S., Martens, A.A., Neves, J.H., Machado-Santelli, G.M., 2014. The multiple facets of drug resistance: one history, different approaches. J. Exp. Clin. Cancer Res. 33, 37.

Northfelt, D.W., Martin, F.J., Working, P., Volberding, P.A., Russell, J., Newman, M., Amantea, M.A., Kaplan, L.D., 1996. Doxorubicin encapsulated in liposomes containing surface-bound polyethylene glycol: pharmacokinetics, tumor localization, and safety in patients with AIDS-related Kaposi's sarcoma. J. Clin. Pharmacol. 36, 55-63.

Provenzano, P.P., Eliceiri, K.W., Campbell, J.M., Inman, D.R., White, J.G., Keely, P.J., 2006. Collagen reorganization at the tumor-stromal interface facilitates local invasion. BMC Med. 4, 38.

Qiu, L., Chen, T., Ocsoy, I., Yasun, E., Wu, C., Zhu, G., You, M., Han, D., Jiang, J., Yu, R., Tan, W., 2015. A cell-targeted, size-photocontrollable, nuclear-uptake nanodrug delivery system for drug-resistant cancer therapy. Nano Lett. 15, 457-463.

Slingerland, M., Guchelaar, H.J., Gelderblom, H., 2012. Liposomal drug formulations in cancer therapy: 15 years along the road. Drug Discov. Today 17, 160-166.

Stylianopoulos, T., Martin, J.D., Chauhan, V.P., Jain, S.R., Diop-Frimpong, B., Bardeesy, N., Smith, B.L., Ferrone, C.R., Hornicek, F.J., Boucher, Y., Munn, L.L., Jain, R.K., 2012. Causes, consequences, and remedies for growth-

633 induced solid stress in murine and human tumors. Proc. Natl. Acad. Sci. U S
634 A. 109, 15101-15108.
635 Swain, S.M., Whaley, F.S., Ewer, M.S., 2003. Congestive heart failure in patients
636 treated with doxorubicin: a retrospective analysis of three trials. Cancer 97,
637 2869-2879.
638 Symon, Z., Peyser, A., Tzemach, D., Lyass, O., Sucher, E., Shezen, E., Gabizon, A.,
639 1999. Selective delivery of doxorubicin to patients with breast carcinoma
640 metastases by stealth liposomes. Cancer 86, 72-78.
641 Szebeni, J., Bedocs, P., Rozsnyay, Z., Weiszhár, Z., Urbanics, R., Rosivall, L., Cohen,
642 R., Garbuzenko, O., Báthori, G., Tóth, M., Bünger, R., Barenholz, Y., 2012.
643 Liposome-induced complement activation and related cardiopulmonary
644 distress in pigs: factors promoting reactogenicity of Doxil and AmBisome.
645 Nanomedicine. 8, 176-84.
646 Takara, K., Hatakeyama, H., Kibria, G., Ohga, N., Hida, K., Harashima, H., 2012.
647 Size-controlled, dual-ligand modified liposomes that target the tumor
648 vasculature show promise for use in drug-resistant cancer therapy. J. Control.
649 Release 162, 225-232.

Figure Captions

Fig. 1. Therapeutic effect of DOX loaded PEG-LP in mice bearing different types of drug-resistant tumors. Mice bearing MDA-MB-231 tumors (A-D) and H69AR (E-F) were treated with 2 mg/kg DOX in PEG-LP or with PBS (control). Data are presented as the mean ± SD (n =4-5). Statistical analysis was done by two-tail Unpaired Student t-test. **P < 0.01; *P < 0.05; N.S., not significant.

Fig. 2. The sensitivities of cancer cells to DOX. The MDA-MB-231 (A) and Hela (B) cells were incubated with different concentrations of DOX for 8 h followed by reincubation for 16 h in the presence of fresh media. The viability of cells (DOX concentration leading to 50% cell-death, EC_{50}) was determined by following the WST-8 assay protocol (n=3). The MDA-MB-231 cells exhibited resistance to DOX, where the Hela cells were found to be sensitive to DOX.

Fig. 3. The cytotoxic effect of free DOX and DOX loaded PEG-LP. A. MDA-MB-231 cells were incubated with different concentrations of DOX for 8 h followed by reincubation for 16 h in the presence of fresh media. The viability of cells (the DOX concentrations leading to 50% cell-death, EC_{50}) was determined by following the WST-8 assay protocol (n=3). Compared to PEG-LP (DOX), free DOX exhibited a better cytotoxic effect. B. Effect of DOX on the morphology of MDA-MB-231 cells. Cells were incubated with either free DOX or DOX loaded PEG-LPs at 37^{o}C. In *in vitro* culture conditions, free DOX (red) dramatically changes the morphology as well as induces the apoptosis of cells compared to PEG-LP (DOX). Scale bars 20 μm.

Fig. 4. Time dependent distribution of DOX delivered by PEG-LPs. MDA-MB-231 cells were incubated with either free DOX or DOX loaded PEG-LP (50 μg DOX/ml) for 3 h at 37^{o}C, followed by washing and reincubation with fresh media for an additional 20 h, followed by rewashing and reincubation with fresh media for an additional 32 h. Images at 3 h, 23 h and 55 h were taken by CLSM. Red: DOX, Blue: Nucleus.

Fig. 5. The mRNA expression levels of various genes in the MDA-MB-231 and OSRC-2 tumors analyzed by real-time PCR. The mRNA expression level of CD31 (vascular endothelial cells marker) in OSRC-2 tumors was higher than that of the MDA-MB-231 tumors. The mRNA expression levels of genes associated with the extracellular matrix (ECM) molecules such as collagen (Col1a1), pericytes (NG2), cancer-associated fibroblasts (Fapα), platelet-derived growth factor receptor protein (Pdgfrb) were up-regulated in MDA-MB-231 tumors than those in OSRC-2 tumors. The mRNA expression levels were normalized to GAPDH (A), NG2 expression level was normalized to CD31 (B). **p<0.01 versus OSRC-2 tumors, unpaired student's t-test.

Fig. 6. Distribution of PEG-LP in MDA-MB-231 and OSRC-2 tumor tissues. Mice bearing MDA-MB-231 tumor (A) and OSRC-2 tumor (B) were injected with rhodamine labeled PEG-LP (0.5 μmol lipid/mouse), or with PBS (Control). Representative images of tumors collected at 24 h post-injection (MDA-MB-231 tumor) or 6 h post-injection (OSRC tumor) are shown, green: tumor vessel, red: PEG-LP, blue: nulcei. PEG-LP was mostly found around the vessels in MDA-MB-231 tumor where it merged (yellow); where as in OSRC-2 tumor, PEG-LP was distributed to deep tumor tissue. Scale bars 50 μm. Distribution of PEG-LP observed at 24 h post-injection in OSRC-2 tumors was also presented in Fig. S1. Furthermore, we reported the distribution of PEG-LP in OSRC-2 tumors in our previously published article (Kibria et al., 2013).

Fig. 7. Site of action and the anti-angiogenic effect of DOX loaded PEG-LP in tumors. A. Mice bearing MDA-MB-231 tumors were treated with 2 mg/kg DOX in PEG-LP or with PBS (Control). At 24 h post-injection, the tumors were collected and analyzed by CLSM. To detect apoptosis in tumors, the mice were injected with an Apo-Trace solution, green: tumor vessel, red: doxorubicin (DOX), blue: apoptotic cells. The total area of the tumor blood vessels (B) were counted from at least 10 images taken from different positions in the tumor/treated group.

Fig. 8. Schematic representation of the mechanism of action of DOX loaded PEG-LP in different types of drug-resistant tumors. In the hyperpermeable tumor (OSRC-

712 2, renal cell carcinoma), PEG-LP (DOX) extravasates to deep tumor tissues via the
713 EPR effect where it delivers DOX to the DOX-resistant tumor cells, therefore PEG-LP
714 (DOX) fails to provide an anti-tumor effect. In contrast, the presence of higher amounts
715 of pericytes, collagen fibers, fibroblasts, platelet-derived growth factor (PDGF) receptor
716 protein makes the MDA-MB-231 tumors hypopermeable, which, in turn, limits the
717 penetration and distribution of PEG-LP (DOX) around the tumor vasculature, and such
718 an effect induces passive anti-angiogenesis, thereby having an effect on life-support
719 (oxygen, nutrients, growth factors etc.) in the drug-resistant tumor.
720

Fig. 1

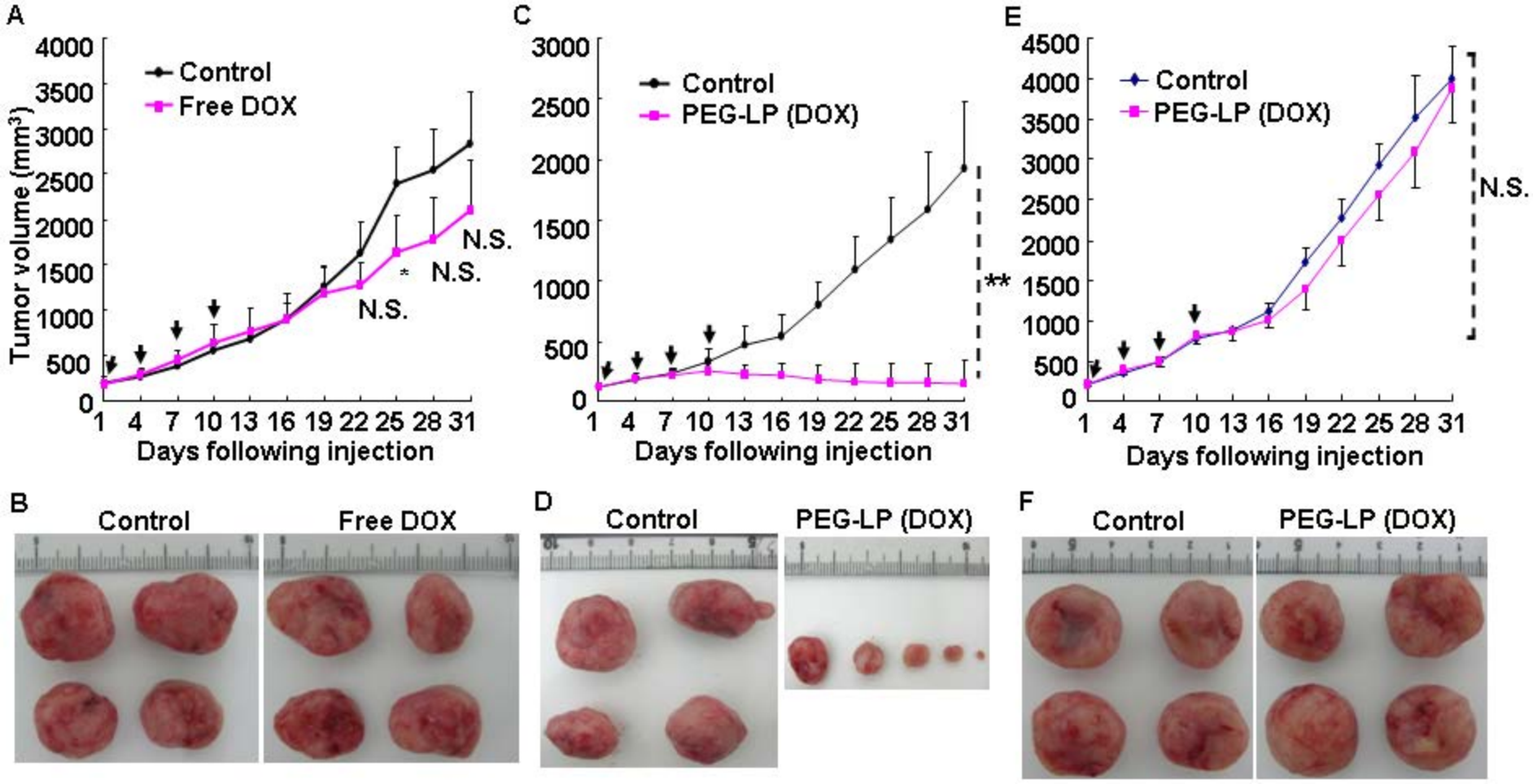
A
Control
Free DOX
Tumor volume (mm3)
Days following injection
N.S.
*
N.S.
N.S.
C
Control
PEG-LP (DOX)
Days following injection
**
E
Control
PEG-LP (DOX)
Days following injection
N.S.
B
Control
Free DOX
D
Control
PEG-LP (DOX)
F
Control
PEG-LP (DOX)

Fig. 2

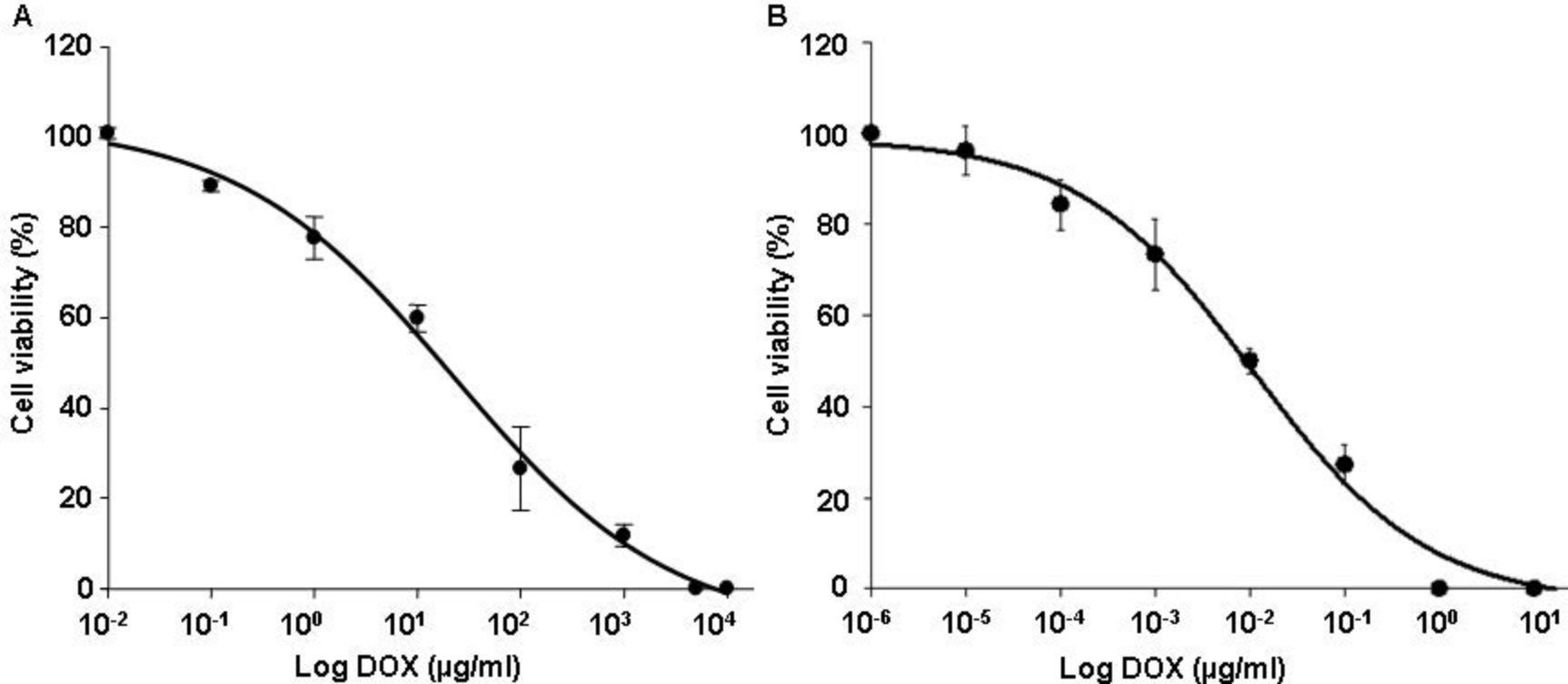
A
120
100
80
60
40
20
0
Cell viability (%)
10-2
10-1
100
101
102
103
104
Log DOX (μg/ml)
B
120
100
80
60
40
20
0
Cell viability (%)
10-6
10-5
10-4
10-3
10-2
10-1
100
101
Log DOX (μg/ml)

Fig. 3

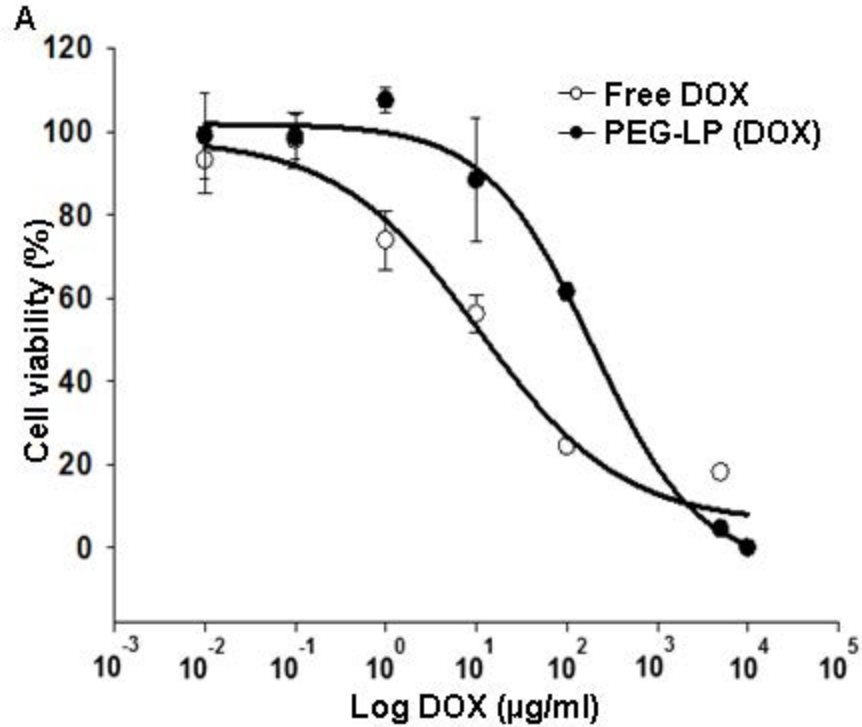
A
120
100
80
60
40
20
0
Cell viability (%)
Free DOX
PEG-LP (DOX)
10^-3
10^-2
10^-1
10^0
10^1
10^2
10^3
10^4
10^5
Log DOX (μg/ml)

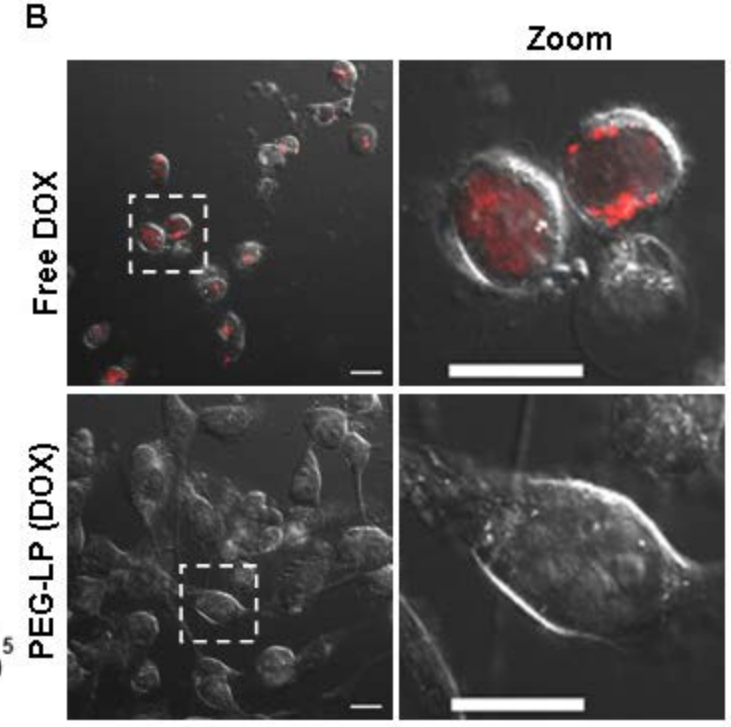
B
Zoom
Free DOX
PEG-LP (DOX)

Fig. 4

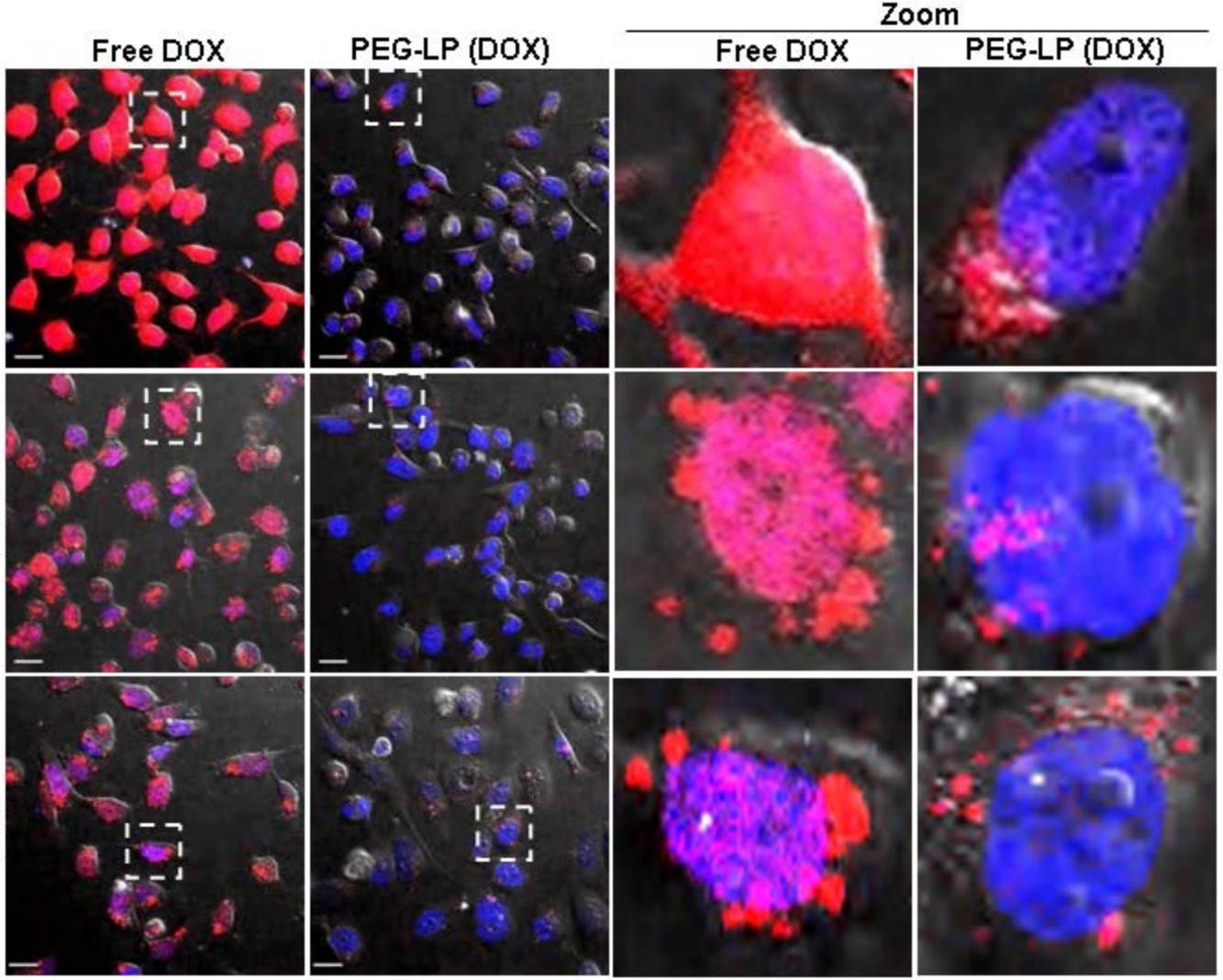

Fig. 5

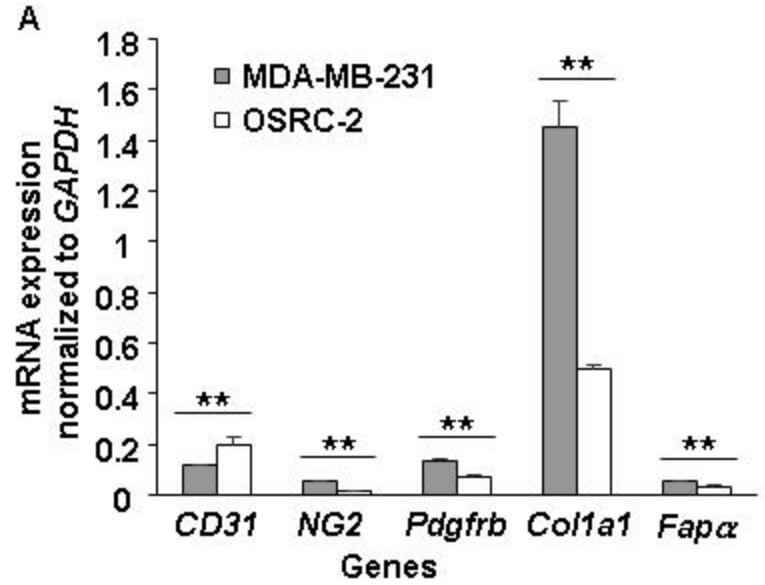
A
mRNA expression normalized to GAPDH
MDA-MB-231
OSRC-2
1.8
1.6
1.4
1.2
1
0.8
0.6
0.4
0.2
0
**
**
**
**
**
CD31
NG2
Pdgfrb
Col1a1
Fapα
Genes

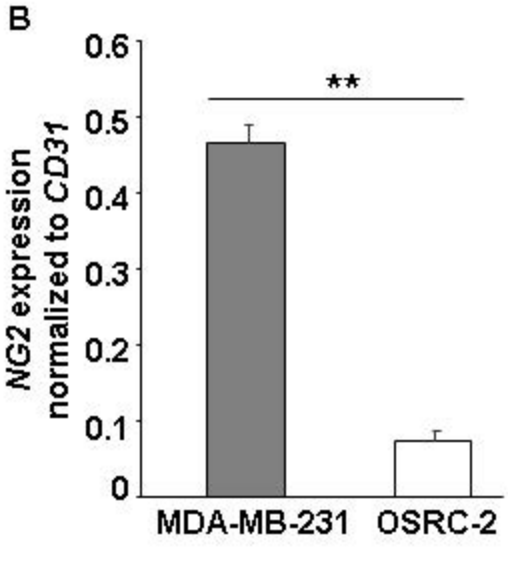
B
NG2 expression normalized to CD31
0.6
0.5
0.4
0.3
0.2
0.1
0
**
MDA-MB-231
OSRC-2

Fig. 6

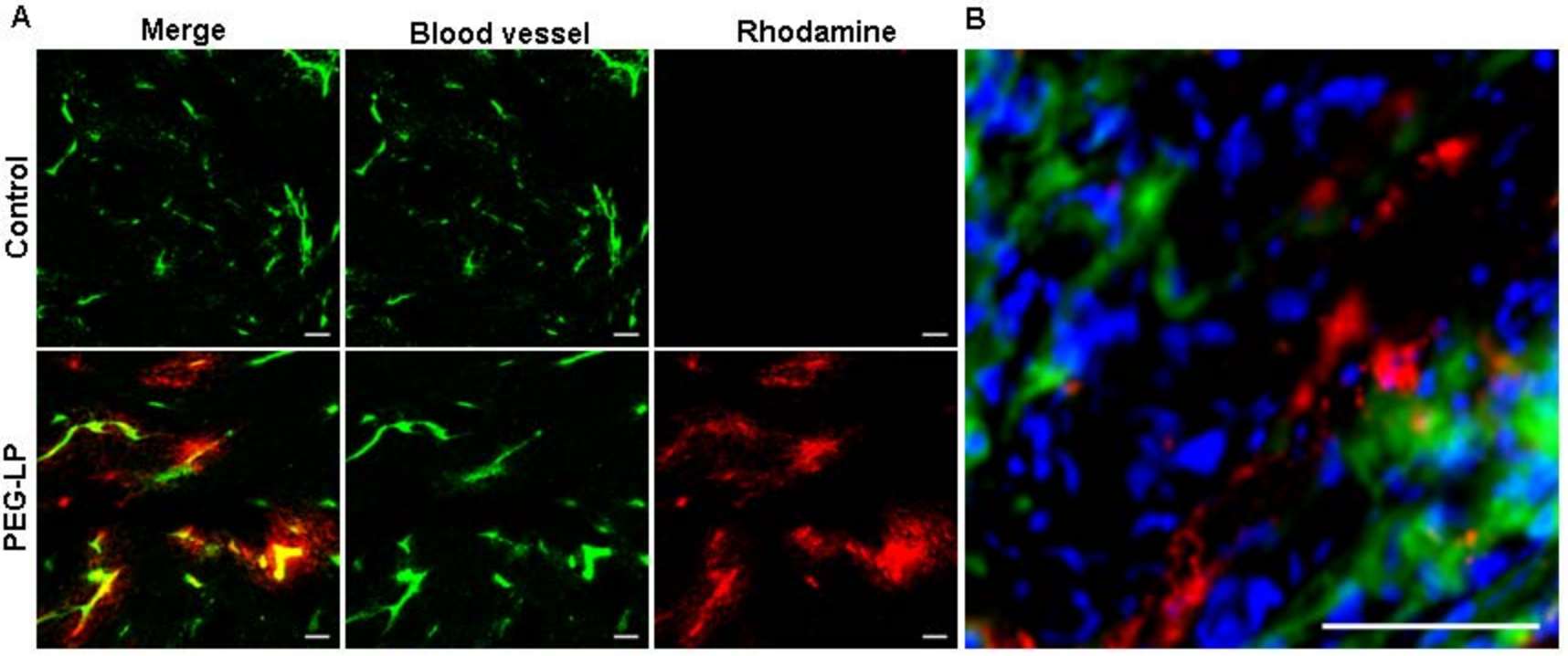

Fig. 7

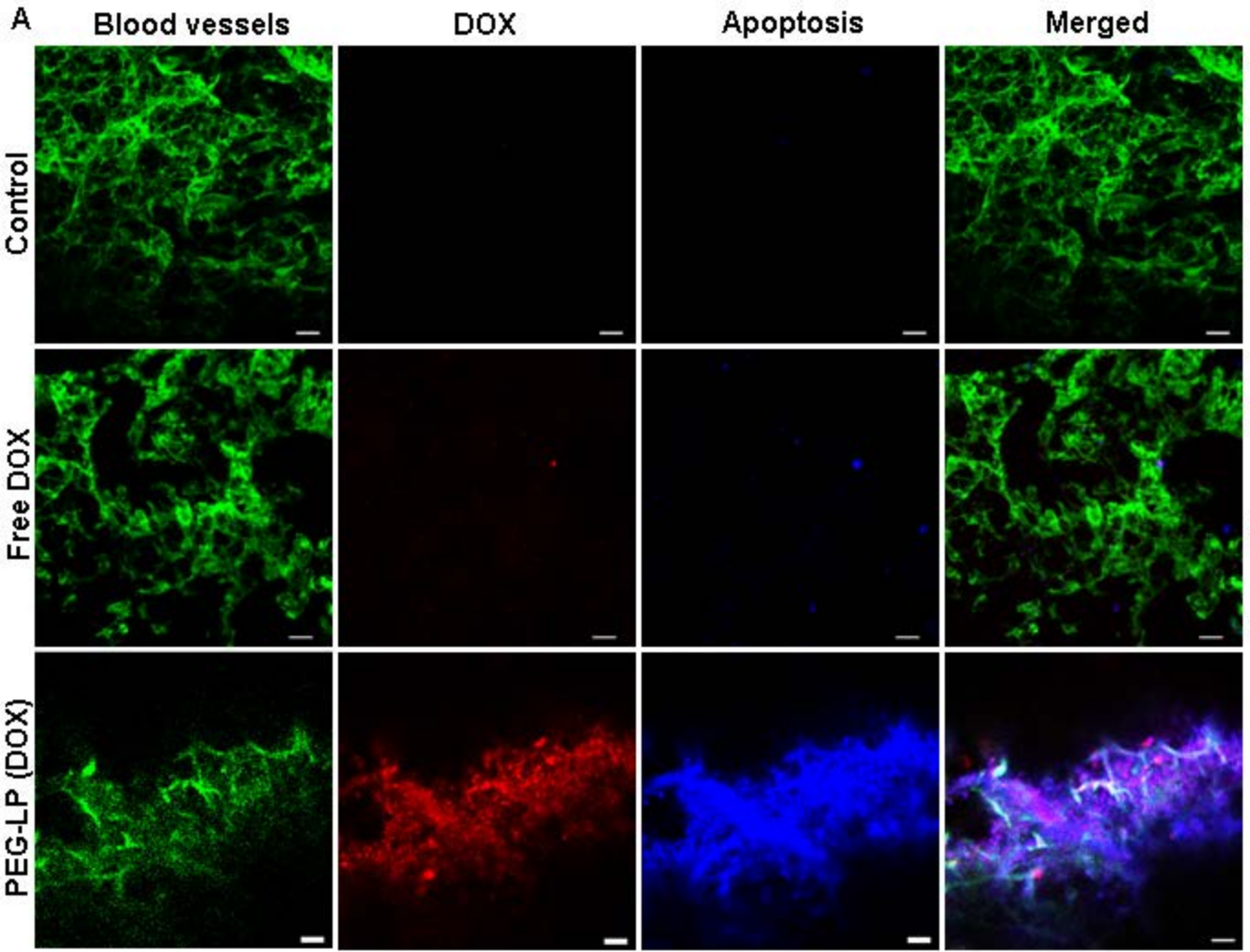
A
Blood vessels
DOX
Apoptosis
Merged
Control
Free DOX
PEG-LP (DOX)

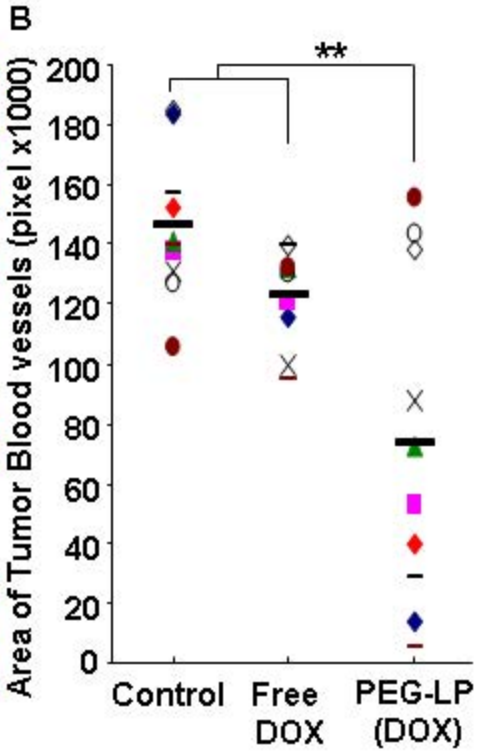
B
**
Area of Tumor Blood vessels (pixel x1000)
200
180
160
140
120
100
80
60
40
20
0
Control
Free DOX
PEG-LP (DOX)

Fig. 8

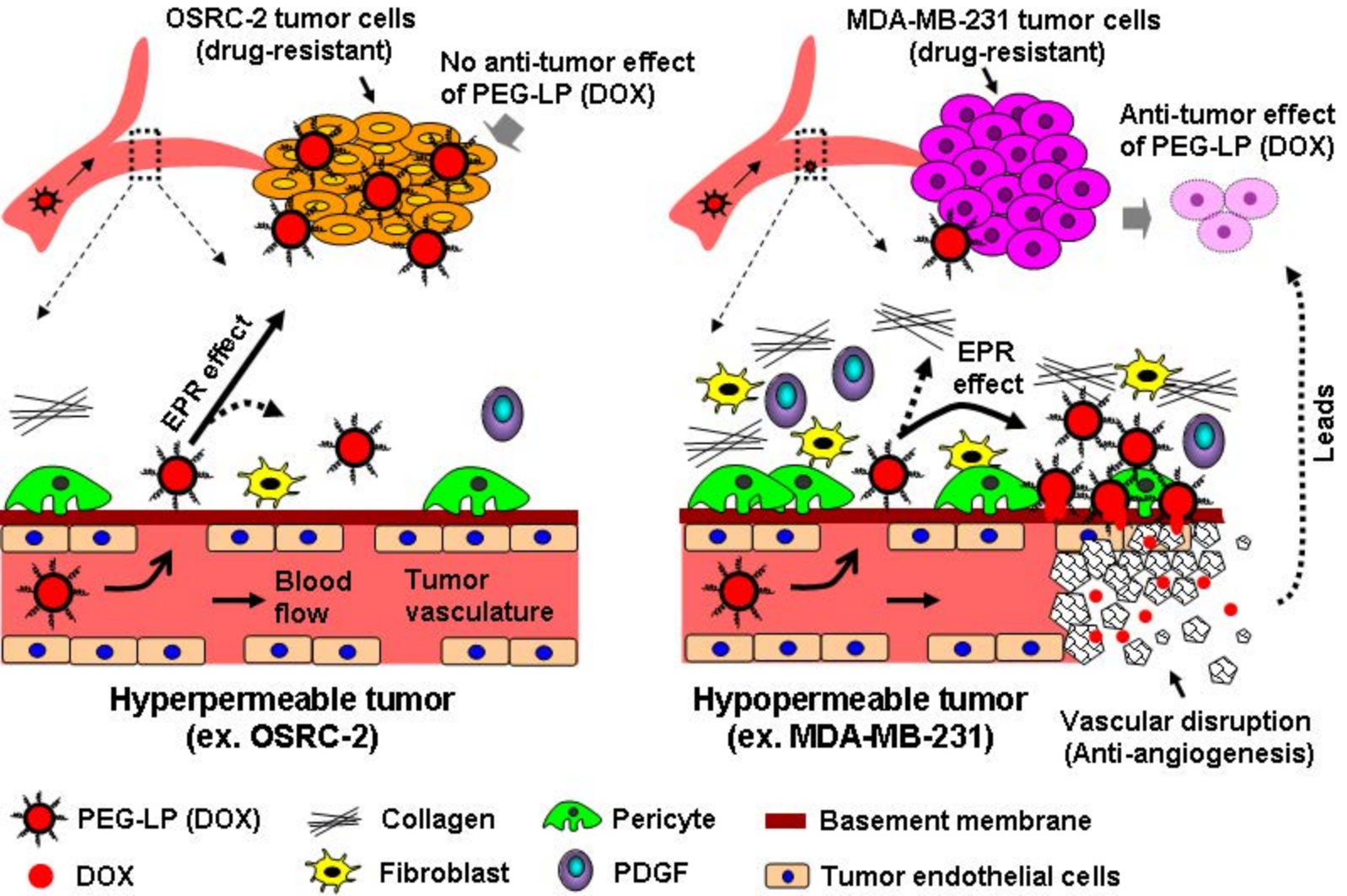
OSRC-2 tumor cells
(drug-resistant)
No anti-tumor effect
of PEG-LP (DOX)
EPR effect
Blood
flow
Tumor
vasculature
Hyperpermeable tumor
(ex. OSRC-2)
MDA-MB-231 tumor cells
(drug-resistant)
Anti-tumor effect
of PEG-LP (DOX)
EPR
effect
Leads
Hypopermeable tumor
(ex. MDA-MB-231)
Vascular disruption
(Anti-angiogenesis)
PEG-LP (DOX)
DOX
Collagen
Fibroblast
Pericyte
PDGF
Basement membrane
Tumor endothelial cells